Glutamine 132 in the NAD(H)-Binding Component of Proton-Translocating Transhydrogenase Tethers the Nucleotides before Hydride Transfer†

Gijs I. van Boxel, Philip G. Quirk, Nick P. J. Cotton, Scott A. White, and J. Baz Jackson*

School of Biosciences, University of Birmingham, Edgbaston, Birmingham B15 2TT, U.K.

Received October 18, 2002; Revised Manuscript Received December 9, 2002

ABSTRACT: Transhydrogenase, found in bacterial membranes and inner mitochondrial membranes of animal cells, couples the redox reaction between NAD(H) and NADP(H) to proton translocation. In this work, the invariant Gln132 in the NAD(H)-binding component (dI) of the *Rhodospirillum rubrum* transhydrogenase was substituted with Asn (to give dI.Q132N). Mixtures of the mutant protein and the NADP(H)-binding component (dIII) of the enzyme readily produced an asymmetric complex, $(dI.Q132N)_2dIII_1$. The X-ray structure of the complex revealed specific changes in the interaction between bound nicotinamide nucleotides and the protein at the hydride transfer site. The first-order rate constant of the redox reaction between nucleotides bound to $(dI.Q132N)_2dIII_1$ was <1% of that for the wild-type complex, and the deuterium isotope effect was significantly decreased. The nucleotide binding properties of the dI component in the complex were asymmetrically affected by the Gln-to-Asn mutation. In intact, membrane-bound transhydrogenase, the substitution completely abolished all catalytic activity. The results suggest that Gln132 in the wild-type enzyme behaves as a "tether" or a "tie" in the mutual positioning of the (dihydro)-nicotinamide rings of NAD(H) and NADP(H) for hydride transfer during the conformational changes that are coupled to the translocation of protons across the membrane. This ensures that hydride transfer is properly gated and does not take place in the absence of proton translocation.

Transhydrogenase couples the stereospecific transfer of hydride ion equivalents between NAD(H) and NADP(H) to proton translocation across a membrane (for recent reviews, see refs *1* and *2*).

$$NADH + NADP^+ + H^+_{out} \Leftrightarrow NAD^+ + NADPH + H^+_{in} \quad (1)$$

Experimentally, for example, in artificial phospholipid membranes, the redox reaction catalyzed by transhydrogenase can either generate or be driven by a proton electrochemical gradient (*3*, *4*). In the cytoplasmic membranes of bacteria and in the mitochondrial membranes of animal cells, the enzyme is usually driven from left to right (eq 1) by the proton gradient developed through the action of the respiratory (or sometimes photosynthetic) electron transport chains (*5*−*7*). In understanding the mechanism of action of transhydrogenase, the central problem is explaining how the pathways of the redox reaction and proton translocation are linked. There is, of course, an equivalent problem for all other coupled solute (or ion) translocators, and in general, the mechanisms of action of this class of enzyme are quite poorly understood. Two experimental demonstrations (a) that there is no intrinsic hydrogen exchange between reduced nucleotide and solvent water during enzyme turnover (*8*) and (b) that the transfer of hydride ion equivalents between nucleotides is direct (*9*) together indicate that the protonation and deprotonation steps involved in translocation are not intimately associated with the redox chemistry of transhydrogenase. There is now a broad consensus that, as in some other solute/ion translocators, protein (and nucleotide) conformational changes are responsible for energy transmission. Our working model, which is supported by much experimental data, is that transhydrogenase is driven between "open" and "occluded" states by protonation from the outside and deprotonation to the inside aqueous phases (*1*). In the open state, nucleotide substrates bind and nucleotide products dissociate, but the redox reaction is prohibited. In the occluded state, the redox reaction is permitted but exchange of bound $NADP^+$ or NADPH with the solvent is blocked. Prevention of the redox reaction in the open state is crucial in this model, but the nicotinamide and dihydronicotinamide rings of the nucleotides are highly reactive; they must therefore be kept apart in the open state and then brought together in the conformational changes, leading to the formation of the occluded state.

The NAD^+/NADH-binding site and the $NADP^+$/NADPH-binding site are located in different structural components of transhydrogenase (Figure 1) known as dI[1] and dIII, respectively, and protrude from the same side of the membrane (e.g., the cytoplasmic side in bacteria). Another component (dII), which is responsible for proton translocation, spans the membrane probably in 12−14 hydrophobic

† We are grateful to the Wellcome Trust, the Biotechnology and Biological Sciences Research Council, and the European Synchrotron Radiation Facility for financial support.

* To whom correspondence should be addressed. E-mail: j.b.jackson@bham.ac.uk.

[1] Abbreviations: $AcPdAD^+$, acetylpyridine adenine dinucleotide (oxidized form); dI, NAD(H)-binding component of transhydrogenase; dIII, NADP(H)-binding component of transhydrogenase; dII, membrane-spanning component of transhydrogenase.

10.1021/bi027032e CCC: $25.00
Published on Web 01/16/2003

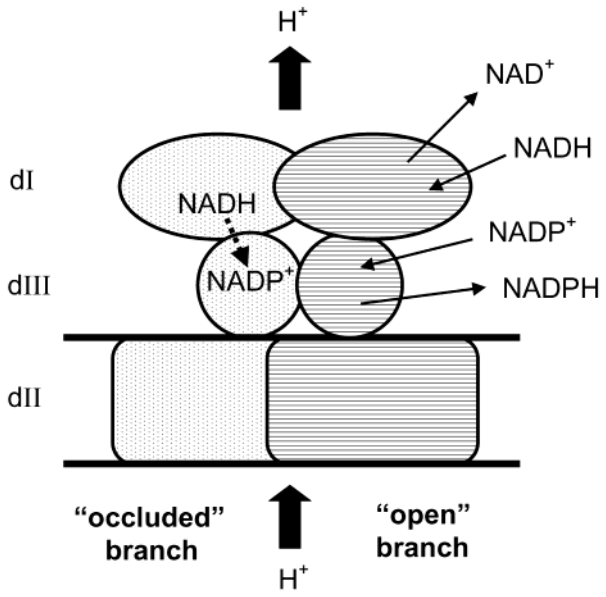

FIGURE 1: Cartoon structure of intact transhydrogenase. The different shadings illustrate site alternation. At the instant that is shown, the right-hand unit (horizontal shading) is in the open conformation, exchanging new substrates for products (thin arrows), and the left-hand unit (dotted shading) is in the occluded conformation, catalyzing hydride transfer (dashed arrow). The direction of proton translocation is shown by the thick arrows.

helices (the number depending on the species). The intact enzyme is essentially dimeric, although there are variations in polypeptide composition in different species. The dI and dIII components have been isolated as stable, water-soluble proteins from transhydrogenases of several species; these proteins bind their cognate nucleotides and interact to form a complex in which the redox reaction can proceed at a very rapid rate (*10*−*14*). The publication of the crystal structure of a complex of the dI and dIII components of *Rhodospirillum rubrum* transhydrogenase (*15*) followed those of isolated *R. rubrum* dI in its NAD^+ form (*16*), isolated bovine (*17*) and human (*18*) dIII in their $NADP^+$ forms, and a solution (NMR) structure of isolated *R. rubrum* dIII (*19*). The very recently determined crystal structure of *R. rubrum* dI in its NADH form (*20*) is remarkably similar to that of dI.NAD^+ (*16*) but exhibits interesting differences of detail. The structures have provided valuable information about how conformational changes might be involved in the shift between the open and occluded states of the enzyme, how the rates of exchange of bound nucleotides with the solvent might be controlled, and how movements of the nicotinamide rings of the nucleotides might regulate hydride transfer. The asymmetry of the complex suggests that, in the intact enzyme, the catalytic sites in the two halves of the dimer alternate during turnover (*15*). An invariant glutamine residue in the "RQD loop" of dI (Gln132 in the *R. rubrum* enzyme) has contacts with both NAD^+ and $NADP^+$ in the crystal structure of the dI_2dIII_1 complex. It is suggested that it might play a key role in the mutual approach of the redox-active C4 atoms of the nicotinamide and dihydronicotinamide rings to constrain the trajectory for the formation of the transition state for hydride transfer. In the work described in this report, the hypothesis is investigated using the *R. rubrum* dI protein in which Gln132 is replaced with an asparagine residue.

MATERIALS AND METHODS

Recombinant dI and dIII and its mutant dIII.E155W from *R. rubrum* transhydrogenase were expressed from plasmids pCD1 (*21*), pNIC2 (*22*), and pJDV1 (*23*), respectively, in appropriate strains of *Escherichia coli* after induction with isopropyl thiogalactoside. The proteins were purified from the harvested cells by column chromatography and stored, as described in those reports. An extra final step on a Q-Sepharose HP column (20 cm × 2.6 cm, Amersham) in 20 mM Tris-HCl (pH 8.0) and 1.0 mM dithiothreitol, to bind the remaining contaminating proteins, was routinely included in all the dI preparations.

Plasmid pCD1 was subjected to site-directed mutagenesis using the Stratagene Quikchange kit and DNA primers supplied by AltaBioscience (5′-GCC GCG CCA ACT CGA TGG ACA TCC TTT CCA GCC-3′ and its complement). After DNA sequencing had been carried out to confirm there were no errors introduced by the PCR, the new plasmid, pGVB1, harboring the gene encoding dI.Q132N, was used to transform cells of *E. coli* C600. As described above, the cells were grown and the protein was purified; elution profiles during chromatography were very similar to those for wild-type dI. Because of the inactivity of dI.Q132N (see the Results), fractions were selected during column chromatography by analysis using SDS−PAGE; the enriched fractions could easily be detected from the intense, Brilliant Blue-stained band at ~40 kDa. As with the wild-type protein (*24*), the molecular mass of the purified product, revealed by gel-exclusion chromatography under nondenaturing conditions on a HiLoad Superdex 200 column (62 cm × 2.6 cm, Amersham), was approximately 82 kDa; the molecular mass of the dI monomer predicted from amino acid sequence is 40.3 kDa. Typically, 250 mg of pure protein were obtained from 3.0 L of bacterial culture. The protein concentration was determined by the microtannin procedure (*25*) and is expressed as dI monomers unless otherwise stated.

Before they were used, the dI proteins were thawed on ice and either used directly or concentrated in Vivaspin centrifugal filters (10 kDa cutoff). Similarly thawed dIII proteins were used directly or were concentrated in 5 kDa cutoff filters, or if indicated, they were treated completely to oxidize their bound nucleotide or to replace it with NADPH (*9*).

Cultures of *R. rubrum* were grown under phototrophic conditions, and inside-out cytoplasmic membranes (chromatophores) were prepared from harvested cells, and stored, as described previously (*26*). The bacteriochlorophyll content of the membranes was determined at 880 nm using an in vivo extinction coefficient of 140 mM^{-1} cm^{-1} (*27*). The dI component was washed from the membranes by centrifugation (*26*).

The extent of steady-state "reverse" transhydrogenation was measured at 25 °C as the reduction of $AcPdAD^+$ by NADPH following the absorbance change at 375 nm in a Perkin-Elmer λ16 apparatus using an extinction coefficient of 6.1 mM^{-1} cm^{-1}. Similarly, the extent of "cyclic" transhydrogenation was measured as the reduction of $AcPdAD^+$ by NADH and $NADP^+$.

Isothermal titration calorimetry experiments were performed on a Microcal MCS instrument at 20 °C and were analyzed using ORIGIN software as supplied by the manu-

facturer. Purified proteins were concentrated by filtration (see above) and then dialyzed for 3 h against 20 mM Hepes (pH 8.0), 10 mM $(NH_4)_2SO_4$, and 1 mM dithiothreitol at 4 °C.

Fluorescence measurements were carried out using a Spex FluoroMax apparatus. Emission spectra of dI.Q132N (1.14 μM) were recorded in 20 mM Hepes, 10 mM $(NH_4)_2SO_4$, and 1 mM dithiothreitol (pH 8.0) at 25 °C with 280 nm excitation. Both slits were set to give half-peak widths of 4 nm. The effect of NADH and NADPH on Trp72 fluorescence was determined in time-drive experiments with 280 nm excitation and 310 nm emission. Nucleotide additions were made sequentially after baseline stability had been established. Primary and secondary inner-filter effects were calculated using 9,10-diphenylanthracene fluorescence and subtracted from the raw data as described previously (*28*). The K_d value for NADH was determined using the program FIG.P.

Stopped-flow experiments were carried out using an Applied Photophysics DX-17MV instrument in either the absorbance or fluorescence mode. The mixing dead time of the instrument was 1.31 ms (*29*). The reduction of $AcPdAD^+$ by NADPH was assessed in absorbance mode at 375 nm (5 nm slits, 2 mm optical path length) during stopped flow after 1:1 mixing. The reduction of $NADP^+$ by NADH was assessed in fluorescence mode. The excitation light was at 280 nm (selected with the instrument's monochromator, 9.3 nm slits), and the emission was collected through a WG305 cutoff filter. Previous experiments with dI_2dIII_1 have shown that fluorescence changes from Trp155 in dIII.E155W are dominant under these conditions; changes from nucleotides and from Trp72 in dI are insignificant (*30*). The kinetics of NADH binding to 1.0 μM dI.Q132N (in the presence and absence of bound NAD^+) were determined from the fluorescence change of Trp72 during stopped flow (*30*). [4B-^{2}H]NADPH (and control [4B-^{1}H]NADPH) were prepared using deuterated (or undeuterated) glucose, hexokinase, and glucose-6-phosphate dehydrogenase, and were purified, as described previously (*31*).

^{1}H NMR spectra of isolated dI.Q132N (560 μM) were recorded at 27 °C on a Bruker AMX500 spectrometer equipped with a cryoprobe. The buffer was 10 mM [^{2}H]-Tris-HCl (pH 7.6), 10 mM $(NH_4)_2SO_4$, 1.0 mM dithiothreitol, and 0.25% NaN_3 in D_2O. Pulse and collect spectra with water presaturation were acquired using an 11 ppm spectral width and comprised 64 transients of 16K data points with a total acquisition time of 2.5 min.

The $(dI.Q132N)_2dIII_1$ complex was crystallized from equimolar solutions of dI.Q132N and wild-type dIII in its $NADP^+$-bound form, essentially as described previously (*15*). The crystals (approximately 100 μm × 100 μm × 100 μm) took 4 days to reach full size. A complete data set was collected to 2.4 Å on an ADSC detector on beamline ID14-4 at the European Synchrotron Radiation Facility at Grenoble, France (see Table 1). The crystals were isomorphous with those of the wild-type dI_2dIII_1 complex. The data were integrated and scaled using the programs MOSFLM (*32*) and SCALA (*33*). Initially, the wild-type structure was refined against the structure factor amplitudes of the mutant crystal using the program CNS (*34*, *35*) and the rigid-body, simulated annealing and geometry minimization protocols before adjusting the model to accommodate the mutation. The structure was further refined using the program REFMAC5 (*36*). The refinement characteristics are summarized in Table 1. This compound appears as Protein Data Bank entry 1NM5.

Table 1: Data Collection and Refinement Statistics for X-ray Crystallography

data collection statistics[a]	
resolution (Å)	30−2.4 (2.53−2.40)
completeness (%)	95.3 (93.4)
multiplicity	2.9 (2.7)
$I/\sigma(I)$	17.8 (1.7)
no. of observations	120855 (15572)
no. of unique reflections	41317 (5828)
R_{sym}[b]	6.0 (55.1)
refinement statistics	
Wilson *B*/average *B*	57/43
no. of non-H atoms/waters	6794/69
rmsd[c] for bonds (Å)/angles (deg)	0.011/1.325
Ramachandran[d]	91.6, 8.1, 0.0, 0.3
R/R_{free}[e]	23.6%/26.4%

[a] Data in parentheses are for the highest-resolution shell. [b] Where $R_{sym} = \sum_j|\langle I\rangle - I_j|/\sum\langle I\rangle$, where I_j is the intensity of the *j*th reflection and $\langle I\rangle$ is the average intensity. [c] Root-mean-square deviation from ideal values. [d] Values are the percentages of amino acids in the core, allowed, generously allowed, and disallowed regions, respectively. [e] Five percent of the data have been set aside for cross-validation calculations.

Cartoon structures were prepared using the program MOLSCRIPT (*37*).

RESULTS

Strong Inhibition of Hydride Transfer in Transhydrogenase by the Q132N Substitution in dI. The recombinant dI protein from *R. rubrum* transhydrogenase in which Gln132 was replaced with an Asn residue (dI.Q132N) was expressed in *E. coli* cells and purified. Like wild-type dI, the hydrodynamic properties of which have been studied in detail (*24*), it ran as a dimer during gel-exclusion chromatography.

The native dI component can be removed from the transhydrogenase of inverted cytoplasmic membranes of *R. rubrum* by washing (*26*, *38*); this organism is one of a group of bacteria in which dI exists as a separate polypeptide (cf. the transhydrogenases of *E. coli* and mammalian mitochondria). Upon re-addition of purified, recombinant dI to the depleted *R. rubrum* membranes (still embedded with the native dII and dIII components), activity is completely restored (*21*) (see Figure 2). However, addition of purified dI.Q132N to dI-depleted membranes did not restore transhydrogenation activity. The same result was obtained even at 2.0 mM $AcPdAD^+$ (data not shown); note that for membranes reconstituted with wild-type dI, the K_m for $AcPdAD^+$ is approximately 100 μM (*39*). When depleted membranes were partially reconstituted with wild-type dI, further addition of dI.Q132N led to inhibition of transhydrogenation, showing that the mutant protein can compete for binding sites; the inactivity of mutant dI is not a consequence of its inability to bind to the dII and dIII components. The relative binding affinities of wild-type and mutant dI for depleted membranes cannot be determined from the data because the extent of monomer exchange between the two dimers ("scrambling") during the assay is not known.

Separately prepared, wild-type dI and dIII readily form a dI_2dIII_1 complex when they are mixed (*21*). The complex catalyzes steady-state forward and reverse transhydrogenation (see eq 1) only very slowly; the reactions are strongly limited

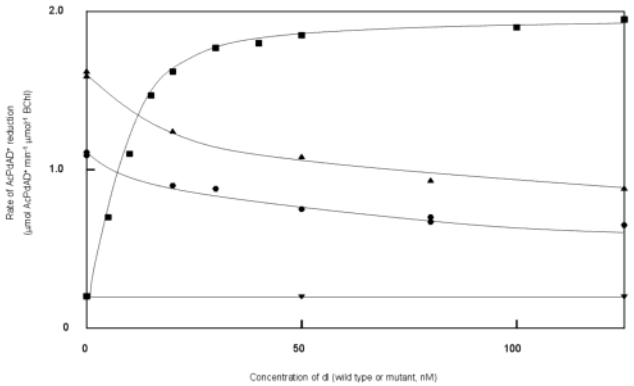

FIGURE 2: Reconstitution of dI-depleted membranes of *R. rubrum* with wild-type recombinant dI and with dI.Q132N. The dI-depleted membranes were suspended in 50 mM Mops, 50 mM KCl, and 2 mM $MgCl_2$ (pH 7.2) supplemented with 200 μM NADPH and 200 μM $AcPdAD^+$, to give a bacteriochlorophyll concentration of 10 μM. The steady-state rate of $AcPdAD^+$ reduction was measured after addition of the dI protein as described in Materials and Methods. The titration was performed with recombinant wild-type dI (■), with dI.Q132N (▼), with dI.Q132N in the presence of 10 nM wild-type dI (▲), and with dI.Q132N in the presence of 20 nM wild-type dI (●).

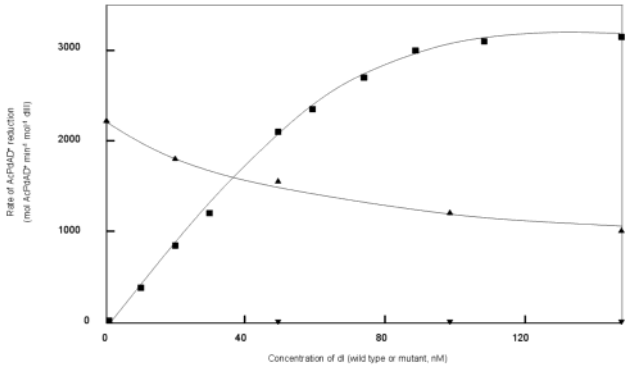

FIGURE 3: Cyclic transhydrogenation in complexes of dIII and either wild-type dI or dI.Q132N. Reactions were carried out in 50 mM Mops, 50 mM KCl, and 2 mM $MgCl_2$ (pH 7.2) supplemented with 200 μM NADH and 200 μM $AcPdAD^+$. The cyclic reaction was supported by the tightly bound NADP(H) on dIII. The dIII concentration was 36 nM in all experiments. The titration was performed with recombinant wild-type dI (■), with dI.Q132N (▼), and with dI.Q132N in the presence of 50 nM wild-type dI (▲).

by low rates of nucleotide product release (NADPH and $NADP^+$, respectively) from dIII. However, wild-type dI_2dIII_1 catalyzes very rapid cyclic transhydrogenation, the reduction of the NAD^+ analogue, $AcPdAD^+$, by NADH in the presence of $NADP^+$ or NADPH. Mechanistically, cyclic transhydrogenation is the sequential oxidation of NADPH by $AcPdAD^+$ and re-reduction of $NADP^+$ by NADH, both of which can take place without NADP(H) leaving the protein. Mixtures of dI.Q132N and wild-type dIII failed to catalyze any detectable cyclic transhydrogenation (Figure 3). However, the presence of dI.Q132N resulted in the inhibition of cyclic transhydrogenation catalyzed by the wild-type dI_2dIII_1 complex, suggesting (see above) that the inactivity of the mutant is not a consequence of a failure in its binding to dIII.

The interaction between dI.Q132N and dIII was studied in more detail using isothermal titration calorimetry (Figure 4). As for wild-type proteins (*24*), the heat changes titrated to an abrupt end point of approximately 2 mol of dI.Q132N

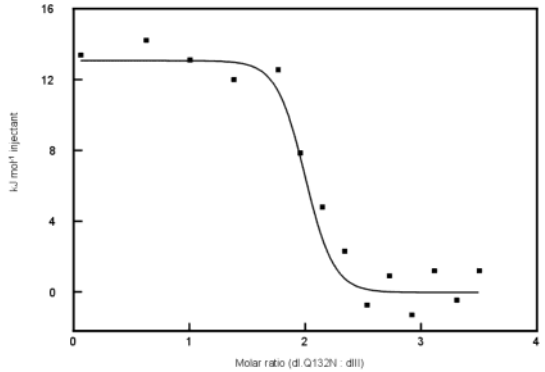

FIGURE 4: Enthalpy changes accompanying the binding of dI.Q132N to wild-type dIII. The calorimeter cell contained 4.2 μM dIII ($NADP^+$ form) and the injection syringe 350 μM dI.Q132N. Each data point corresponds to a single injection (1 × 1.0 μL, followed by 19 × 3.0 μL) separated by 210 s.

per mol of dIII, indicating the formation of a stable $(dI.Q132N)_2dIII_1$ heterotrimer. The enthalpy change was ~13 kJ/mol of dIII (compared with ~11 kJ/mol of dIII measured in wild-type dI−dIII titrations). ORIGIN indicated a K_d of ≈60 nM for dissociation of the complex into monomers of dIII and dimers of dI.Q132N, but this is probably too low for a meaningful comparison with that of the dI_2dIII_1 complex [for which we estimated a K_d of ≤60 nM (*24*)].

Studies of the transient-state kinetics of dI_2dIII_1 complexes have provided a valuable approach toward understanding the redox reaction of transhydrogenase. Stopped-flow experiments with wild-type dI_2dIII_1 complexes revealed a rapid, single-turnover burst of $AcPdAD^+$ reduction by NADPH prior to the onset of the very slow steady-state reaction (*31*) (see Figure 5a). When the concentration of dI dimers is sufficient to saturate dIII, the apparent first-order rate constant of the monoexponential burst ($k_{app} \approx 600\ s^{-1}$) corresponds to that of hydride transfer and the associated conformational changes. The reduction of $AcPdAD^+$ by NADPH catalyzed by $(dI.Q132N)_2dIII_1$ complexes also displayed approximately monoexponential burst kinetics but with a greatly decreased k_{app} (~200-fold) (Figure 5b). As with dI_2dIII_1, the amplitude of the burst was equivalent to approximately 60% of a single turnover of $AcPdAD^+$ reduction, and this is a reflection of the perturbed on-enzyme equilibrium constant, as discussed previously (*40*). The concentration of $AcPdAD^+$ required to give the half-maximal value of k_{app} (approximately 2 mM) was ~10-fold larger than in experiments with the wild-type dI_2dIII_1 complexes (Figure 5d). The experiments shown in traces a and b of Figure 5 were carried out with the protein complex loaded with NADPH in one syringe and $AcPdAD^+$ in the other before mixing. Parallel experiments with dIII.NADPH in one syringe and dI.Q132N and $AcPdAD^+$ in the other gave similar reaction kinetics (data not shown). This indicates that neither the association of dI with dIII nor the binding of $AcPdAD^+$ to dI limits the rate of the reaction. With wild-type dI_2dIII_1, there is a modest primary deuterium isotope effect on the k_{app} for the burst of $AcPdAD^+$ reduction when $NADP^1H$ is replaced with $NADP^2H$ (deuterium at the 4-*pro-S* position of the dihydronicotinamide ring): $k_H/k_D = 2.0 \pm 0.1$ at 20 °C (*31*). However, the deuterium isotope effect was insignificant for $(dI.Q132N)_2dIII_1$ complexes ($k_H/k_D = 1.1 \pm 0.1$ at 20 °C), suggesting a change in the rate-limiting step of the reaction (see the Discussion).

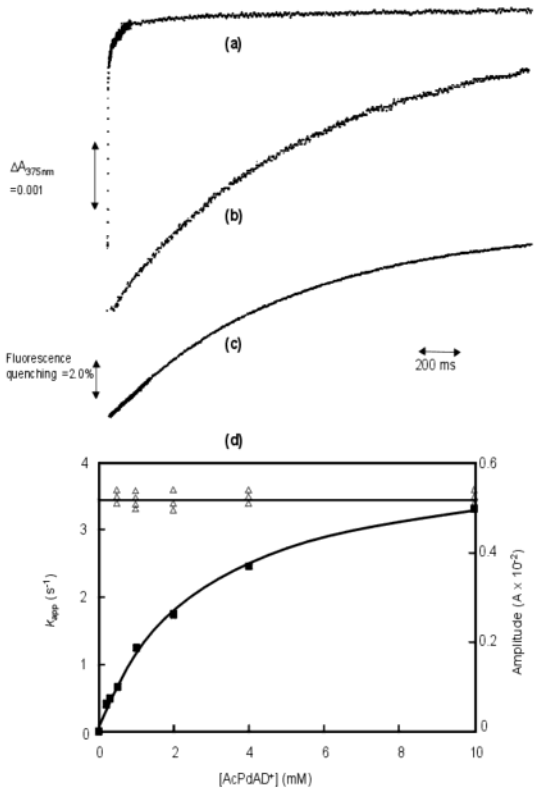

FIGURE 5: Stopped-flow kinetics of hydride transfer in complexes of dI and dIII. Experiments were performed in 20 mM Hepes, 10 mM $(NH_4)_2SO_4$, and 1 mM dithiothreitol (pH 8.0) at 20 °C. Proteins were prepared as described previously (*30*). For the experiment shown in trace a, the first syringe contained 100 μM dI and 50 μM dIII.NADPH and the second 2 mM AcPdAD$^+$, before mixing. The trace is an average of six absorbance recordings at 375 nm after 1:1 mixing. The experiment in trace b is similar except that dI.Q132N was used in place of wild-type dI. For trace c, the experiment was performed in fluorescence mode (see Materials and Methods) with the first syringe containing 100 μM dI.Q132N and 50 μM dIII.E155W in its NADP$^+$ form and the second containing 200 μM NADH. The trace, an average of six recordings after 1:1 mixing, shows the quenching of Trp155 fluorescence as bound NADP$^+$ is reduced (see the text). In comparable experiments under similar conditions, but with wild-type dI, the reaction was complete within the mixing time (and see refs *30* and *41*). Panel d shows the dependence of the apparent first-order rate constant (■) and amplitude (△) of the reaction burst upon the concentration of AcPdAD$^+$, carried out under the conditions described for trace b.

Because of the overlapping absorbance bands of NAD(H) and NADP(H), it is difficult to measure directly the rates of the redox reaction between the two physiological substrates of transhydrogenase. However, the thermodynamic and catalytic properties of *R. rubrum* dIII.E155W (in complex with dI) are very similar to those of wild-type dIII, and usefully, the fluorescence emission of the introduced (lone) Trp residue reports on the nucleotide occupancy of the protein; the fluorescence is high when NADP$^+$ is bound and low when NADPH is bound (*30*). Thus, we can monitor the transient-state kinetics of the redox reaction catalyzed by $dI_2(dIII.E155W)_1$ complexes with the physiological nucleotides from measurements of the Trp155 fluorescence. In complexes with wild-type dI in the forward reaction (bound NADP$^+$ reduced by NADH), the decrease in fluorescence recorded in a continuous flow device yielded a k_{app} for the redox step of 21 200 s^{-1} at saturating nucleotide concentrations (*41*). Figure 5c shows that the rate of this reaction catalyzed by $(dI.Q132N)_2(dIII.E155W)_1$ complexes was very much lower and was easy to measure during stopped flow. Because of interference from nucleotide absorbance, k_{app} could not be measured at high NADH concentrations but the reaction was still far from saturated at 100 μM nucleotide where k_{app} was approximately 2 s^{-1} [compare to 1000 s^{-1} in $dI_2(dIII.E155W)_1$ under similar conditions].

Nucleotide Binding to dI.Q132N and to (dI.Q132N)$_2$dIII$_1$ Complexes. Despite the profound effect of the Q132N substitution on the hydride transfer kinetics, two sets of experiments showed that the mutation had little effect on the NADH binding affinity of isolated protein (Figure 6). In the first, we investigated the NADH-dependent quenching of fluorescence from the single, native Trp of dI at position 72. Note that the unusually short wavelength emission band (310 nm), reflecting the local, nonpolar environment of this Trp residue in the β-sheet of domain dI.1, is identical in the wild type and mutant (data not shown). Now NADPH addition did not lead to Trp fluorescence quenching in dI.Q132N, but titration with NADH had a large effect and gave a single K_d of 20 μM [Figure 6a; compare that with a similar value obtained for the wild-type protein (*21*)]. These values are close to the limit of reliability of this methodology due to the quite large inner-filter effects of the nucleotide and the consequent difficulty in determining the titration end point. However, the second set of experiments, with isothermal titration calorimetry, gave a very similar outcome (Figure 6b). The data fitted well to the algebraic relationship for a single class of binding sites ($K_d = 25$ μM, $n = 1.4$ per protein dimer, $\Delta H = -79.6$ kJ/mol of dimer); compare that with a K_d of 18 μM ($n = 2.0$ per dimer, $\Delta H \approx -123.4$ kJ/mol of dimer) for wild-type dI under similar conditions (*24*). Note that K_d values calculated from these and similar experiments were reproducible and should be reliable. However, because K_d is high relative to the protein concentration, the estimate of the binding stoichiometry (n) is subject to significant error. Nevertheless, it is clear that while dI and dI.Q132N are both dimeric proteins, there are no evident cooperative interactions between the two nucleotide-binding sites.

The on and off rate constants for NADH binding to and release from wild-type dI ($\sim 2 \times 10^7$ M^{-1} s^{-1} and ~ 430 s^{-1}, respectively, at 15.5 °C) and the off rate constant for NAD$^+$ release (~ 1000 s^{-1} at 13.2 °C) were determined from the rates of change of Trp72 fluorescence during stopped flow (*30*). Equivalent experiments with dI.Q132N gave Trp72 fluorescence changes slightly faster than those observed with the wild-type protein. Values of k_{obs} were approximately 2-fold greater at similar temperatures and nucleotide concentrations, taking the measurements close to the operational limits of the instrument (data not shown).

In contrast to the similarity of the results with isolated dI and dI.Q132N, small but significant differences in the NADH binding properties of dI_2dIII_1 and $(dI.Q132N)_2dIII_1$ complexes were observed. Only isothermal titration calorimetry gave satisfactory data with the complex; because higher nucleotide concentrations were needed for saturation, the large inner-filter effects precluded use of Trp fluorescence quenching. Experiments were performed with "dead-end" complexes to block hydride transfer; i.e., NADH was titrated into solutions of dI_2dIII_1 complexes the dIII component of which was in the NADPH form. Wild-type dI_2dIII_1 has two

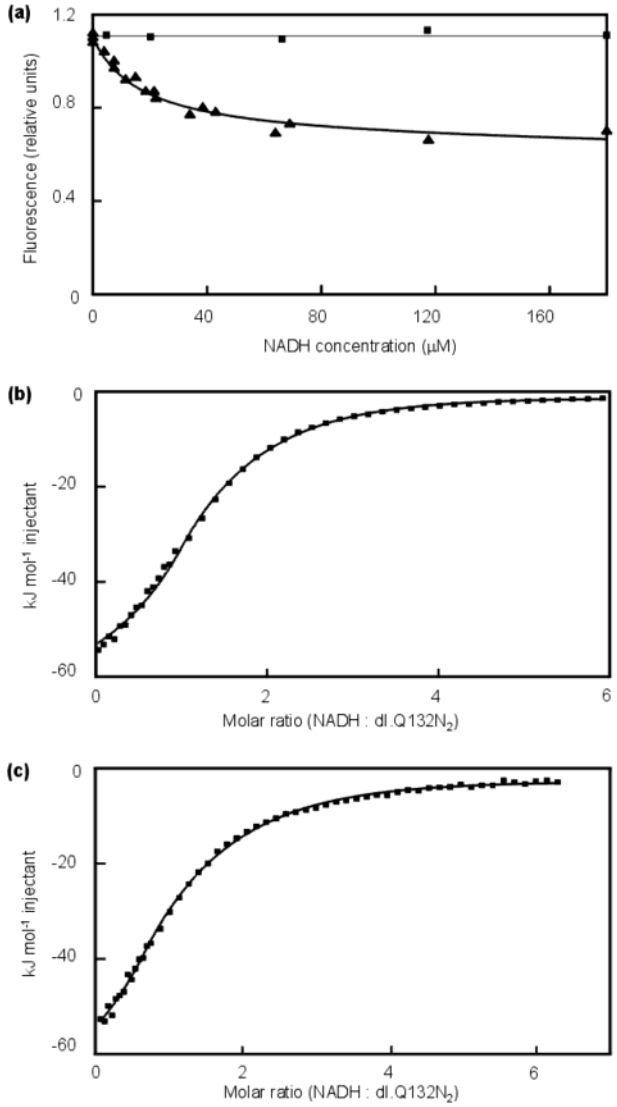

FIGURE 6: Binding of NADH to isolated dI.Q132N and to $(dI.Q132N)_2dIII_1$. (a) Quenching of Trp72 fluorescence. The fluorescence changes in a solution of dI.Q132N upon addition of NAD(P)H were corrected for inner filtering as described in Materials and Methods: (▲) NADH and (■) NADPH. The curve through the NADH data shows a binding isotherm for a K_d of 20 μM calculated by the program FIG.P. (b) Enthalpy changes upon addition of NADH to dI.Q132N. The calorimeter cell contained 147 μM protein and the injection syringe 2.5 mM NADH. Each data point corresponds to a single injection (1 × 1.0 μL, followed by 15 × 2.5 μL and then 29 × 6.0 μL) separated by 210 s. (c) Enthalpy changes upon addition of NADH to $(dI.Q132N)_2dIII_1$. The cell contained 75 μM complex and the injection syringe 2.2 mM NADH. Each data point corresponds to a single injection (1 × 1.0 μL, followed by 15 × 3.0 μL and then 44 × 6.0 μL) separated by 210 s. The curves in panels b and c show the binding isotherms calculated with ORIGIN using parameters given in the text.

classes of binding sites for NADH (*24*). One has a K_d very similar (17 ± 5 μM) to that of the two sites in the isolated dI dimer (see above), and the other has a lower affinity for NADH (the K_d is approximately 300 μM). The isothermal titration calorimetry data for NADH binding to $(dI.Q132N)_2dIII_1$ similarly indicated that there are two classes of sites (the results did not fit satisfactorily to the relationship for a single class of binding sites). A good fit was obtained when the algorithm was set to 1.0 binding site per complex for the first class and 1.0 per complex for the second class of sites; calculated K_d values were 15 and 178 μM (Figure 6c). The affinity of the first site is very similar to that found in dI_2dIII_1, but the titrations reproducibly indicated a higher affinity for the second site than that in the wild-type protein.

$NADP^+$ release and NADPH release from isolated dIII are both extremely slow ($k_{off} \approx 0.03$ and 3×10^{-4} s^{-1}, respectively), and they are even slower (~5-fold) from dI_2dIII_1 complexes (*24*). Measurements of Trp155 fluorescence revealed that the rate of $NADP^+$ release from dIII caused by formation of a complex with dI.Q132N was similar to that produced with wild-type dI (results not shown).

Crystal Structure of $(dI.Q132N)_2dIII_1$ Complexes. In the crystal structure of $(dI.Q132N)_2dIII_1$ complexes, the subunit organization and protein folds are very similar to those described for dI_2dIII_1 (*15*). Following the earlier convention, the two dI.Q132N polypeptides in the complex are designated A and B. Each of these comprises two domains, dI.1 (amino acid residues 1−137 and 328−384) and dI.2 (residues 138−327), separated by a cleft. The RQD loop (residues 126−136) forms part of the cleft lining of dI.1. The dIII polypeptide is positioned at the side of the cleft in the B polypeptide and interacts with the RQD loop and with residues in dI.2 from that subunit; it has only a small surface of contact with the A polypeptide. Thus, the cleft of polypeptide A is not associated with a dIII molecule. NAD^+ binds to the A polypeptide of $(dI.Q132N)_2dIII_1$ in a configuration similar to that observed in dI_2dIII_1; the dI.2 domain serves in the manner of a typical dinucleotide binding site (*42*), and the nicotinamide ring protrudes into the cleft where it interacts with residue 132. The shorter side chain of Asn132 results in a slightly different packing in this region in the mutant and wild-type proteins. An H-bond between Asn132 and the 3-carboxamide that is not evident with Gln132 becomes possible.

The region most affected by the Q132N substitution is in the cleft of polypeptide B where this subunit interfaces with dIII. The most obvious difference is that, even though the two types of crystals were grown at identical nucleotide concentrations, the NAD^+ electron density is much stronger in $(dI.Q132N)_2dIII_1$ than in dI_2dIII_1 and defines the nucleotide more clearly. The electron density of the adenosine part of the NAD^+ in the B polypeptide of $(dI.Q132N)_2dIII_1$ is good and reveals very close conformational similarities with the nucleotide in the A polypeptide. However, the NMN moiety is in weak density, suggesting a substantial degree of disorder. This finding echoes that made on the binding site of isolated *R. rubrum* dI, where the nucleotide adopts *syn*, *anti*, and disordered conformations in different subunits of the asymmetric unit (*16*). Close to the NAD^+ in polypeptide B resides the $NADP^+$ in dIII. The conformations of dIII and its bound $NADP^+$ are quite similar in the dI_2dIII_1 and $(dI.Q132N)_2dIII_1$ crystal structures; the nucleotide adopts the unusual "reversed" orientation (relative to that found in the classical Rossmann fold), as described previously (*19*). As in polypeptide A, the side chain of Asn132 in polypeptide B is in good electron density, but in this region, we can identify what might be an important difference with the structure of dI_2dIII_1. In the wild-type complex, Gln132 from polypeptide B extends across the subunit interface such that its amide group can make H-bond contact with the 2′-hydroxyl of the *N*-ribose of the bound $NADP^+$ (Figure 7a).

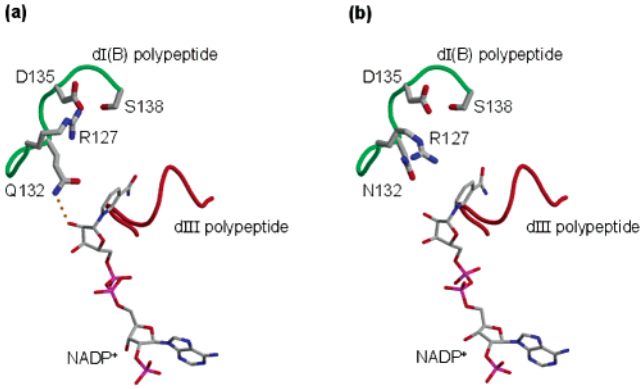

FIGURE 7: Comparison of the X-ray structures of (a) the wild-type dI_2dIII_1 complex and (b) the $(dI.Q132N)_2dIII_1$ complex in the region of the interface between the RQD loop and the $NADP^+$-binding loop. The dI(B) polypeptide from residue 125 to 140 is shown in green, and the dIII polypeptide from residue 81 to 96 is shown in red. Amino acid side chains and $NADP^+$ are shown in conventional atom colors. The dotted yellow line in panel a shows an H-bond between Gln132 and the 2′-hydroxyl of the nicotinamide ribose of the bound $NADP^+$.

Table 2: Chemical Shifts of H Atoms in Amino Acid Side Chains of Wild-Type dI and dI.Q132N[a]

	chemical shift (ppm)			chemical shift (ppm)	
residue	dI	dI.Q132N	residue	dI	dI.Q132N
Thr228/Thr231	1.21	1.21	Met226	2.06	2.05
Ala384	1.33	1.33	MetD	2.07	2.07
Ala236	1.36	1.37	Tyr235	6.82, 7.11	6.82, 7.12
Met239	1.96	1.96	Phe243	7.20, 7.31	7.20, 7.32
MetB	2.04	2.04			

[a] The basis for the assignments of wild-type dI is described (*43*). MetB and MetD are identified only on the basis of their chemical shifts.

In the crystal structure of the mutant complex, because of the shorter side chain of Asn132, the formation of this H-bond is not possible (Figure 7b).

Residues 223−239 in dI of *R. rubrum* transhydrogenase form a "mobile loop" with a highly conserved GYA motif at its apex. The feature emanates from dI.2 on the side of the cleft opposite the RQD loop. The electron density of the mobile loop in available X-ray structures is somewhat variable. It is most clearly defined in isolated dI where, in one subunit, it comes to within ∼8 Å of Gln132. The side chain protons of amino acid residues in the mobile loop of isolated dI are easily resolved in NMR experiments (*43*). The slow relaxation that results from the segmental mobility of the loop gives relatively narrow resonances versus those of others in the protein which are broadened by the long correlation time of the molecule as a whole (its dimeric molecular mass is 80.6 kDa). The ^1H NMR spectrum of dI.Q132N in the absence of nucleotides (i.e., with the loop in its mobile state) was very similar to that of wild-type dI; there were no detectable changes in the chemical shifts of the assigned residues (Table 2). The addition of NADH [to either dI (*43*) or dI.Q132N, results not shown] resulted in the broadening of resonances from residues in the loop due to its closing down on the surface of the protein. The nucleotide concentration dependences of the resonance broadening, known to correlate with NADH binding, were similar in the two proteins, supporting conclusions reached above.

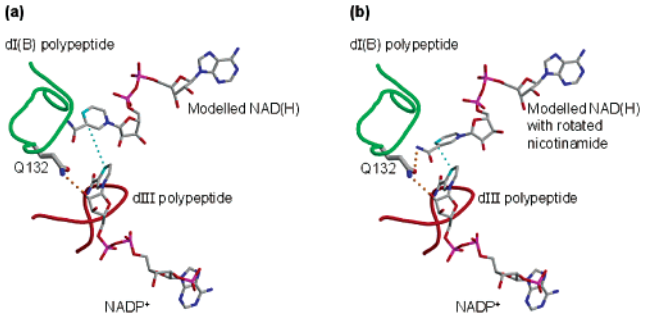

FIGURE 8: Modeled NADH in (a) the nucleotide-distal and (b) the nucleotide-proximal conformations of the dI_2dIII_1 complex. From the crystal structures of the dI_2dIII_1 complex, the dI(B) polypeptide from residue 125 to 140 is shown in green and the dIII polypeptide from residue 86 to 96 is shown in red. Into panel a is modeled an NAD(H) molecule; it has the same conformation as the NAD^+ in polypeptide dI(A) and is inserted into an equivalent site (see the text). In panel b, the PA−O3, O5S−C5S, C5S−C4S, and C1S−N1N bonds of the NAD(H) are rotated by 20°, 20°, 35°, and 19°, respectively (see the text). Amino acid side chains and $NADP^+$ are shown in conventional atom colors except for the NC4 atoms of the nucleotides, which are pale blue. The dotted yellow lines represent H-bonds (see the text). The pale blue dotted lines indicate distances between the NC4 atoms of the nucleotides: 6.5 Å in panel a and 3.4 Å in panel b.

DISCUSSION

The single dIII component in the dI_2dIII_1 complex is locked in the occluded state; it can catalyze very rapid hydride transfer between its bound nucleotide and the nucleotide bound to the dI(B) polypeptide, and it can exchange $NADP^+$ and NADPH with the solvent only very slowly (*1*). (After hydride transfer in the intact enzyme, interactions with dII during proton translocation would shift the dIII into its open state to prohibit further redox reaction and permit fast nucleotide exchange.) During hydride transfer in the occluded state, for example, in forward transhydrogenation (eq 1), the C4 atoms of the dihydronicotinamide ring of NADH and the nicotinamide ring of $NADP^+$ must be brought into apposition (*9*). Perhaps because crystallization is carried out with catalytically dead-end complexes (i.e., both nucleotides oxidized to prevent redox chemistry), this configuration is not observed in any of the X-ray structures, and the pretransition state for hydride transfer has to be modeled (Figure 8). Figure 8a depicts the crystal structure of the dI_2dIII_1 complex at the interface between the dI(B) polypeptide and dIII. There are two important features for the present discussion. First, the *re* face of the $NADP^+$ nicotinamide ring packs against residues in the binding loop on dIII, and second, the side chain of Gln132 from dI(B) extends across the protein interface to make H-bond contact with the 2′-hydroxyl group of the *N*-ribose of the $NADP^+$. Other important residues at the catalytic site were pointed out (*15*). Into this structure we have modeled an NAD(H) molecule in a similar conformation and in the site equivalent to that of the NAD^+ in the dI(A) polypeptide (which is in good density). However, in this modeled structure, the C4 atom of the NADH (were the nucleotide in its reduced form) and the C4 atom of the $NADP^+$ would be some 6.5 Å apart; in conflict with the experimental observation, this distance would be too great for rapid, direct hydride transfer between the nucleotides. Now in the asymmetric unit of isolated dI crystals, the NAD^+ in two of the four polypeptides adopts

different conformations; with the adenosine moiety remaining relatively fixed in its binding pocket, the nicotinamide is rotated in and out of the cleft between domains dI.1 and dI.2 (*16*) (the nicotinamide rings in the other two polypeptides are in weak electron density). In Figure 8b, the dihydronicotinamide of the modeled NADH in the dI_2dIII_1 complex is rotated by movements equivalent to those seen in isolated dI, from the "distal position" into a "proximal position", in which its C4-H group is in van der Waals contact with C4 of the $NADP^+$ nicotinamide. We suggest that this approximates the ground state from which direct hydride transfer is initiated. In this conformation of the nucleotides, the 3-carboxamide group of the NADH can make an H-bond with the side chain amide of Gln132, thus stabilizing the proximal position of the nucleotides. Through the H-bonds to the $NADP^+$ *N*-ribose and the NADH 3-carboxamide, residue Gln132 would act as a molecular tether for maintaining the dihydro- and nicotinamide rings at an appropriate distance for the formation of the transition state for the redox reaction. Note that hydride transfer will proceed from the *pro-R* hydrogen of the NC4 of NADH to the *si* face of the NC4 of $NADP^+$, giving the well-known A-to-B stereochemistry (*8*, *44*). In principle, further constraints, e.g., ring puckering to activate the pseudoaxial positions of the C4 atoms of the rings in the transition state [as calculated for NAD(P)(H)-linked dehydrogenases (*45*)], might also be imposed by the interactions promoted by the Gln132 tether.

The crystal structures show that shortening the Gln132 side chain by one methylene group in the dI.Q132N mutant is sufficient to break the H-bond with the 2′-hydroxyl of the $NADP^+$ *N*-ribose across the dI(B)−dIII interface (Figure 7b). This results in a failure of the tether; the dihydronicotinamide ring of the NADH and the nicotinamide ring of the $NADP^+$ are not readily maintained in the proximal position, and the rate of hydride transfer is greatly decreased. The distal position might, in fact, be stabilized in the catalytic site of the mutant by the formation of the "new" H-bond between Asn132 and the 3-carboxamide of NAD^+, as seen in the structure of the A polypeptide. Note that the loss of the H-bond between Asn132 and the $NADP^+$ *N*-ribose does not lead to a significant change in the position of the $NADP^+$ in its binding site in the $(dI.Q132N)_2dIII_1$ crystal structure. Thus, in the wild-type protein, the $NADP^+$ *N*-ribose forms an anchor point for the tether; having bound to this group, the other "arm" of Gln132 (carbonyl or amino, we cannot distinguish at this resolution) captures the NADH 3-carboxamide. Other factors that might contribute to the inhibition of hydride transfer in the Q132 mutant can be considered. The loss of the H-bond between Gln132 and the $NADP^+$ *N*-ribose will, in itself, have little effect on the reactivity of the nicotinamide ring. Changes in the postulated H-bond organization between Gln132/Asn132 and the carboxamide group of the NAD(H) nicotinamide, through an effect on electron withdrawal from the ring, might influence the rates of hydride transfer, but this is unlikely to be significant: (a) 3-Acetylpyridine adenine dinucleotide ($AcPdAD^+$) and its reduced form are good substrates for transhydrogenase, and (b) as judged by the amplitude of the burst of hydride transfer (Figure 5), the replacement of Gln132 with Asn does not greatly affect the equilibrium constant of this step.

We should consider the possibility that the distal and proximal conformations of the nucleotides represent intermediates on the reaction coordinate of intact transhydrogenase. Previously, we argued that to ensure tight coupling with proton translocation, the redox reaction must be prevented in the open state and permitted only in the occluded state of the enzyme (*1*); this could be achieved by the relative movements of the dihydronicotinamide ring of NADH and the nicotinamide ring of $NADP^+$. The change in the nucleotide conformation seen in isolated dI seems to be driven by a change in the width of the cleft between domains dI.1 and dI.2 (*16*), and in the intact enzyme, we can envisage this to be the result of alterations in the interaction between the RQD loop of dI.1 and helix D/loop D of dIII (*15*). The measured change in the kinetic isotope effect (KIE) of the rate constant for the transient-state burst of $AcPdAD^+$ reduction by NADPH in $(dI.Q132N)_2dIII_1$ complexes provides new evidence for a conformational change associated with the hydride transfer step. The KIE in the wild-type complex, though only modest, indicates that hydride transfer itself is at least partly rate limiting during the single-turnover redox reaction. The much lower KIE in the mutant complex clearly suggests a change in the position of the rate-limiting step. The rates of binding and release of nucleotides from the complex were shown to be barely affected by the mutation (in fact, they slightly increase), and we suggest that a hitherto undetected conformational change associated with hydride transfer must limit the rate of the reaction burst. It is entirely possible that this conformational change corresponds to the much decreased rate of the nucleotide distal−proximal conversion in the 3-actetylpyridine group of the $AcPdAD^+$ caused by the failure of the tether when Gln132 is replaced with Asn. We would conclude that the distal−proximal conversion is $>10^3$ times faster in the wild type than in the mutant.

It was argued that, in intact transhydrogenase, the nucleotide binding site of dI becomes high affinity for NADH and low affinity for NAD^+ as this protein component dissociates from its dIII partner in the formation of the open state; this allows the replacement of product nucleotides with new substrates from the solvent (*15*). Now the *R. rubrum* dI_2dIII_1 complex (in its NADPH-bound form) has a high-affinity and a low-affinity binding site for NADH (*24*). The high-affinity site has a K_d similar to that of the two equivalent NADH-binding sites on the dimer of isolated dI, and it must therefore be located on the polypeptide (polypeptide A) the cleft of which is not occupied by (occluded) dIII. In support of this conclusion, the substitution of Gln132 with Asn had no effect on the K_d for NADH, either of isolated dI or of the high-affinity site on the dI_2dIII_1 complex (Figure 6). Furthermore, the rates of NADH binding and release and of NAD^+ release from isolated dI were affected little by the mutation, and there was no detectable influence on the dynamics of mobile loop closure of isolated dI during titration with NADH (Table 2). It would appear that shortening the side chain of residue 132 by one CH_2 group, while having profound effects in the occluded state of transhydrogenase (see above), does not modify the salient characteristics of the open state. The X-ray structures show that there are differences in the contacts between the nucleotide 3-carboxamide group and the A polypeptide that are caused by the mutation, but evidently these interactions do not greatly affect the overall binding energy.

The electron density of the adenosine moiety of the NAD^+ in the B polypeptide of $(dI.Q132N)_2dIII_1$ is well-defined and reveals ligand−protein interactions similar to those in the A polypeptide, giving some justification to the basis for the nucleotide modeling shown in Figure 8. The density in the NMN region is very weak, supporting the notion of conformational flexibility in this region of the nucleotide while it is bound to the protein. We were unable to assign any electron density to NAD^+ in the B polypeptide of wild-type dI_2dIII_1 (*15*) and attributed this to disorder in the nucleotide structure and/or to the low occupancy of the site; the complexes were crystallized in the presence of NAD^+ and $NADP^+$ (to prevent the redox reaction), and we suggested that Coulombic repulsion between the two positively charged nicotinamide rings interferes with binding (in the complete enzyme, this might limit the formation of catalytically dead-end complexes). Perhaps the somewhat less tightly packed structure in the binding site of $(dI.Q132N)_2dIII_1$ permits more conformational freedom of the NMN moiety of the NAD^+, and this results in a failure to restrict the coincident binding of the two oxidized nucleotides.

In dI_2dIII_1 complexes, NAD^+ and NADH (and their analogues) enter and leave the catalytic site by what is probably an abnormal (though rapid) pathway. Thus, in the intact enzyme, these nucleotides bind to dI when the latter is loosely associated with dIII in an *open* state, but prior to catalysis in the dI_2dIII_1 complex, they bind to a dI that is tightly associated with dIII in an *occluded* state. There are two general procedures available for studying nucleotide interaction with dI at the single catalytic site of the dI_2dIII_1 complex. The first is equilibrium binding in dead-end complexes. It was established that the K_d for NADH of just one site on the dI dimer (that on the B polypeptide) is elevated upon formation of a complex with the dIII.NADPH species (*24*). Consistent with the thesis that only dI associated with an occluded dIII is affected by mutation of Gln132 (see above), only the K_d for this site is altered in $(dI.Q132N)_2dIII_1$ (Figure 6). The measured increase in affinity, here in an NADH−NADPH dead-end complex, probably corresponds to the increased level of occupancy of the B polypeptide seen in the crystal structure of the NAD^+−$NADP^+$ form of $(dI.Q132N)_2dIII_1$ (as discussed above). Second, the interaction of NAD(H) and AcPdAD(H) at the single catalytic site of the dI_2dIII_1 complex can be investigated from the nucleotide concentration dependences of rates under conditions of turnover, most reliably under transient-state conditions. For technical reasons (see the Results), we were able to obtain a full set of data only for the reduction of $AcPdAD^+$ by NADPH. The large increase in the amount of $AcPdAD^+$ required to produce the half-maximal rate in the single-turnover burst of hydride transfer in $(dI.Q132N)_2dIII_1$ relative to dI_2dIII_1 (Figure 5) can be simply explained by the notion that the formation of the proximal conformation of the $AcPdAD^+$ is no longer favored when Gln132 is replaced with an Asn residue.

The work described in this report essentially relates to events taking place at the single catalytic site of dI_2dIII_1 complexes. However, it should not be overlooked that, in the intact enzyme, the two sites of the transhydrogenase dimer probably alternate during turnover (see ref *1* and Figure 1), and currently, there is very little indication as to how the conformational changes in the two halves of the "dimer" are synchronized. Different experimental approaches have led to suggestions that other membrane-located solute translocators operate by alternating-site mechanisms (*46*, *47*). The fact that the dI and dIII components of *R. rubrum* transhydrogenase can be isolated as stable, water-soluble proteins and that they combine into a catalytically active asymmetric complex, the crystal structure of which has now been determined, make it a very attractive experimental system for exploring further the fundamental principles and underlying similarities in this group of membrane transporters.

ACKNOWLEDGMENT

We are grateful to Avtar Singh, Jamie Venning, Klaus Fütterer, and Andy Lovering for very helpful discussion and to Stephanie Monaco for assistance collecting synchrotron X-ray data.

REFERENCES

1. Jackson, J. B., White, S. A., Quirk, P. G., and Venning, J. D. (2002) *Biochemistry 41*, 4173−4185.
2. Bizouarn, T., Fjellstrom, O., Meuller, J., Axelsson, M., Bergkvist, A., Johansson, C., Karlsson, G., and Rydstrom, J. (2000) *Biochim. Biophys. Acta 1457*, 211−218.
3. Rydstrom, J. (1979) *J. Biol. Chem. 254*, 8611−8619.
4. Eytan, G. D., Carlenor, E., and Rydstrom, J. (1990) *J. Biol. Chem. 265*, 12949−12954.
5. Rydstrom, J., and Hoek, J. B. (1988) *Biochem. J. 254*, 1−10.
6. Sazanov, L. A., and Jackson, J. B. (1994) *FEBS Lett. 344*, 109−116.
7. Hickman, J. W., Barber, R. D., Skaar, E. P., and Donohue, T. J. (2002) *J. Bacteriol. 184*, 400−409.
8. Lee, C. P., Simard-Duquesne, N., Ernster, L., and Hoberman, H. D. (1965) *Biochim. Biophys. Acta 105*, 397−409.
9. Venning, J. D., Grimley, R. L., Bizouarn, T., Cotton, N. P. J., and Jackson, J. B. (1997) *J. Biol. Chem. 272*, 27535−27538.
10. Yamaguchi, M., and Hatefi, Y. (1995) *J. Biol. Chem. 270*, 28165−28168.
11. Diggle, C., Bizouarn, T., Cotton, N. P. J., and Jackson, J. B. (1996) *Eur. J. Biochem. 241*, 162−170.
12. Fjellstrom, O., Bizouarn, T., Zhang, J., Rydstrom, J., Venning, J. D., and Jackson, J. B. (1999) *Biochemistry 38*, 415−422.
13. Peake, S. J., Venning, J. D., and Jackson, J. B. (1998) *Biochim. Biophys. Acta 1411*, 159−169.
14. Weston, C. J., Venning, J. D., and Jackson, J. B. (2002) *J. Biol. Chem. 277*, 26163−26170.
15. Cotton, N. P. J., White, S. A., Peake, S. J., McSweeney, S., and Jackson, J. B. (2001) *Structure 9*, 165−176.
16. Buckley, P. A., Jackson, J. B., Schneider, T., White, S. A., Rice, D. W., and Baker, P. J. (2000) *Structure 8*, 809−815.
17. Prasad, G. S., Sridhar, V., Yamaguchi, M., Hatefi, Y., and Stout, C. D. (1999) *Nat. Struct. Biol. 6*, 1126−1131.
18. White, S. A., Peake, S. J., McSweeney, S., Leonard, G., Cotton, N. N. J., and Jackson, J. B. (2000) *Structure 8*, 1−12.
19. Jeeves, M., Smith, K. J., Quirk, P. G., Cotton, N. P. J., and Jackson, J. B. (2000) *Biochim. Biophys. Acta 1459*, 248−257.
20. Prasad, G. S., Wahlberg, M., Sridhar, V., Sundaresan, V., Yamaguchi, M., Hatefi, Y., and Stout, C. D. (2002) *Biochemistry 41*, 12745−12754.
21. Diggle, C., Hutton, M., Jones, G. R., Thomas, C. M., and Jackson, J. B. (1995) *Eur. J. Biochem. 228*, 719−726.
22. Jeeves, M., Smith, K. J., Quirk, P. G., Cotton, N. P. J., and Jackson, J. B. (1999) *J. Biomol. NMR 13*, 305−306.
23. Peake, S. J., Venning, J. D., Cotton, N. P. J., and Jackson, J. B. (1999) *Biochim. Biophys. Acta 1413*, 81−91.
24. Venning, J. D., Rodrigues, D. J., Weston, C. J., Cotton, N. P. J., Quirk, P. G., Errington, N., Finet, S., White, S. A., and Jackson, J. B. (2001) *J. Biol. Chem. 276*, 30678−30685.
25. Mejbaum-Katzenellenbogen, S., and Drobryszycka, W. J. (1959) *Clin. Chim. Acta 4*, 515−522.
26. Cunningham, I. J., Williams, R., Palmer, T., Thomas, C. M., and Jackson, J. B. (1992) *Biochim. Biophys. Acta 1100*, 332−338.

27. Clayton, R. K. (1963) *Biochim. Biophys. Acta 73*, 312−323.
28. Kubista, M., Sjoback, R., Eriksson, S., and Albinsson, B. (1994) *Analyst 119*, 417−419.
29. Tonomura, B., Nakatani, H., Ohnishi, M., Yamaguchi-Ito, J., and Hiromi, K. (1978) *Anal. Biochem. 84*, 370−383.
30. Venning, J. D., Peake, S. J., Quirk, P. G., and Jackson, J. B. (2000) *J. Biol. Chem. 275*, 19490−19497.
31. Venning, J. D., Bizouarn, T., Cotton, N. P. J., Quirk, P. G., and Jackson, J. B. (1998) *Eur. J. Biochem. 257*, 202−209.
32. Leslie, A. G. W. (1992) *Joint CCCP4 and ESF-EADBM Newsletter on Protein Crystallography 226*.
33. Evans, P. R. (1997) *Joint CCP4 and ESF-EACMB Newsletter on Protein Crystallography 33*, 22−24.
34. Brunger, A. T., Adams, P. D., Clore, G. M., Delano, W. L., Gros, P., Grossekunstleve, R. W., Et, A. L., and Warren, G. L. (1998) *Acta Crystalogr. D54*, 905−921.
35. Grosse-Kunstleve, R. W., and Brunger, A. T. (1999) *Acta Crystallogr. D55*, 1568−1577.
36. Murshudov, G. N., Vagin, A. A., and Dodson, E. J. (1997) *Acta Crystallogr. D53*, 240−255.
37. Kraulis, P. J. (1991) *J. Appl. Crystallogr. 24*, 946−950.
38. Fisher, R. R., and Guillory, R. J. (1971) *J. Biol. Chem. 246*, 4679−4686.
39. Gupta, S., Quirk, P. G., Venning, J. D., Slade, J., Bizouarn, T., Grimley, R. L., Cotton, N. P. J., and Jackson, J. B. (1998) *Bochim. Biophys. Acta 1409*, 25−38.
40. Venning, J. D., and Jackson, J. B. (1999) *Biochem. J. 341*, 329−337.
41. Pinheiro, T. J. T., Venning, J. D., and Jackson, J. B. (2001) *J. Biol. Chem. 276*, 44757−44761.
42. Eventoff, W., and Rossmann, M. G. (1975) *CRC Crit. Rev. Biochem. 111*, 111−140.
43. Quirk, P. G., Smith, K. J., Thomas, C. M., and Jackson, J. B. (1999) *Biochim. Biophys. Acta 1412*, 139−148.
44. Fisher, R. R., and Guillory, R. J. (1971) *J. Biol. Chem. 246*, 4687−4693.
45. Almarrson, O., and Bruice, T. C. (1993) *J. Am. Chem. Soc. 115*, 2125−2138.
46. van Veen, H. W., Margolles, A., Muller, M., Higgins, C. F., and Konings, W. N. (2000) *EMBO J. 19*, 2503−2514.
47. Senior, A. E., and Bhagat, S. (1998) *Biochemistry 37*, 831−836.

BI027032E